Title

EFFECT OF POLARIZED X-RAY BEAM IN SMALL ANGLE SCATTERING BY PYROLYTIC GRAPHITE

Author

Biswal, Madan Mohan.

Publication Date

1971-03-01

Thesis/dissertation

UCRL-20517

EFFECT OF POLARIZED X-RAY BEAM IN SMALL ANGLE SCATTERING BY PYROLYTIC GRAPHITE

Madan Mohan Biswal

(M. S. Thesis)

March 1971

AEC Contract No. W-7405-eng-48

LAWRENCE RADIATION LABORATORY
UNIVERSITY of CALIFORNIA BERKELEY

UCRL-20517

DISCLAIMER

EFFECT OF POLARIZED X-RAY IN SMALL ANGLE SCATTERING BY PYROLYTIC GRAPHITE

Madan Mohan Biswal

Inorganic Materials Research Division, Lawrence Radiation Laboratory
Department of Materials Science and Engineering, College of Engineering
University of California, Berkeley, California

Abstract

The effect of a strongly polarized x-ray beam in the small angle scattering of pyrolytic graphite (P.G.) was investigated in three different orientations, in an angular region very close to the direct beam. Strong double Bragg scattering occurred mainly from (0002) layer planes, when the electric vector of the x-ray beam was parallel to these planes. No such effect was observed in the other two orientations. This shows that double Bragg scattering can be eliminated in certain orientations by using a highly polarized beam in small angle scattering. In the ultra small angle region (less than 60 secs of θ), a specimen volume effect on intensity has been confirmed.

TABLES OF CONTENTS

I. INTRODUCTION

A good understanding of the structural characteristic of pyrolytic graphite has already been made by several workers.[1-3] It consists of an oriented aggregate of turbostratic crystallites having unit cell parameters similar to those of carbon blacks and having L_a and L_c dimensions of the order of 100 A.[1] Guentert and Cvikevich[2] have shown pyrolytic graphite to be a polycrystalline material with a high degree of preferred orientation, but with a random layer stacking order. Small angle scattering from this material is well known and the interpretation in terms of density variation, due to voids has been demonstrated.[3]

In the last few years, it has been recognized that most of the small angle scattering from cold worked metals is due to double Bragg reflections which comes from randomly oriented subgrains. In case of pyrolytic graphite because the deposited materials are randomly oriented in the deposition plane in the form of subgrains, it can be expected that an appreciable amount of the small angle scattering is due to double Bragg reflection. Bragg and Packer[3] pointed out that the excess characteristic scattering in one certain orientation in pyrolytic graphite is due to the above mechanism. The above interpretation of the double Bragg phenomenon has been done with data obtained using unpolarized x-ray beam. It was the purpose of this investigation to identify the orientation dependence in double Bragg scattering of pyrolytic graphite by using strongly polarized x-ray beams obtained from the modern small angle scattering apparatus developed on the concept of Bonse and Hart.[4]

Three different orientation of the layer planes have been chosen. As will be demonstrated in the text of this report, the double Bragg scattering exists primarily in one orientation, the electric vector is parallel to the layer planes, but it is not observed in other two orientations.

The second feature of this experimental work was the unexpected appearance of the volume effect in the small angle scattering data in ultra small angular region in P.G. This effect predicted by Warren has not been previously reported experimentally. In order to confirm this effect, two separate experiments were performed with LiF (single crystal) and pure graphite, where the above volume effect was definitely demonstrated. The theory developed by Guinier[5] and Warren[6] for volume effect must be worked out to fully explain these experimental results.

II. INSTRUMENTAL SET UP

The AMR x-ray Low Angle Scattering Goniometer used for this experiment consists of two grooved perfect Ge crystals arranged in parallel position with the sample placed between them. The x-ray beam is multiply diffracted (six times per crystal) by the first crystal and produces a monochromatic primary x-ray beam which has the same physical width as the x-ray source, but exhibits an extremely narrow angular divergence(Fig. 1). The scattered beam from the sample is then analyzed by diffracting it from the second crystal into a suitable detector. The second crystal has the capability of 'seeing' only a very narrow angular divergence, resulting in high resolution. The multiple Bragg reflections, obtained between the walls of the groove results in the effective elimination of the tails of the reflection curve, with only a slight reduction in the peak intensity.[7] (Fig. 2a and 2b). The second crystal is capable of being rotated around the center of the sample by means of a large barrel micrometer calibrated in steps of one second of arc θ.

The peak intensity after 12 reflection can be expressed as,

$$I_{peak} = a^{12} I_o$$

Where, 'a' is the fraction of the incident beam diffracted per reflection. For nearly perfect crystals, a = 0.98; Clearly,

$$I_{peak} = (0.98)^{12} I_o = 0.7\ I_o$$

Thus the peak intensity is decreased by 30% after 12 reflections.

The crystals are designed to diffract CuK_α radiation emitted by a spot rather than a line x-ray source. The walls of the crystal grooves are parallel to the (220) planes of germanium.

A. Familiarization with Beam Shape for Slit Height Correction

Short exposures of the primary beam at the specimen position and after the second crystal at zero angle were made. Typical exposures are reproduced in Fig. 3a and Fig. 4a respectively. The intensity distribution across the equator (perpendicular bisector of the primary beam image) of the film was determined with a microphotometer of scanning area 2 mm× 200 microns, as shown in Fig. 3b and Fig. 4b. From these figures, the finite dimensions of the direct beam cross section imply a distortion of the true diffraction pattern. Since the beam is focussed into a line in the plane of observation, the distortion of the scattering pattern due to beam width is often reduced and neglected. Then the distortion is assumed to be due to the beam height.

The process of correcting experimental scattering curves for collimation errors which will be referred as 'unfolding' has been considered by several authors.[8,9] For slits of negligible width, the experimental scattering intensity F(h) for a scattering angle h, measured at a point P, (Fig. 5) is related to the perfect collimation scattered intensity I(h) by the equation

$$F(h) = \int_0^\infty g(y)\, I\sqrt{(h^2+y^2)}\, dy \qquad (1)$$

where g(y) is a weighting function, the form of which depends on the collimating system. For slits of negligible width and infinite height g(y) = 1.

For most usual case of a radially symmetrical true intensity distribution, I(h) could be found from the relation,

$$I(h) = -\frac{2}{\pi} \int_0^{\infty} \frac{dt}{\sqrt{(h^2+t^2)}} F' \sqrt{h^2 + t^2} \qquad (2)$$

It is generally assumed that the source profile of an x-ray tube can be described by a Gaussian weighting function, then

$$g(y) = \frac{2}{\delta \sqrt{2\pi}} \exp\left(-\frac{y^2}{2\delta^2}\right)$$

$$= \frac{2p}{\sqrt{\pi}} \exp\left(-p^2 y^2\right)$$

'p' is a constant determined by the slit height, clearly $p^2 = 1/2\delta^2$. A small p corresponds to high slits and a large 'p' to small slits. For this weighting function one can obtain I(h) from

$$I(h) = -\frac{\exp\left(p^2h^2\right)}{p^2\sqrt{(\pi)}} \int_0^{\infty} \frac{dt}{\sqrt{(h^2+t^2)}} N' \sqrt{(t^2+h^2)} \qquad (3)$$

where, $N(h) = F(h) \exp\left(-p^2h^2\right)$

and $$N' \sqrt{t^2+h^2} = \frac{dN\sqrt{t^2+h^2}}{d\sqrt{t^2+h^2}}$$

Equation (3) is the general solution of the collimation error problem. In principle it makes possible the correction of the experimental scattering curve by numerical or graphical method.

The function F(h) can be obtained by microphotometering of the diffraction pattern along the film equator in several rows, the numbers of which is determined by the requirements of numerical integration. The function g(y) can be deduced by microphotometering the trace of the primary beam, which will give the shape of the desire function.

B. Recognition that the Beam is Polarized

Whenever crystal monochromatized x-ray radiation is used, the beam is partially polarized owing to the reflection by the monochromator crystal. A six times diffracted beam is therefore polarized even more. Intensity ratio in two orthogonal directions has been derived for diffraction of the crystal monochromatized x-ray beam used in this work, (Appendix A). From this calculation it is seen that the intensity in a perpendicular direc- (z-axis) is much stronger (68 times) than in the plane of incidence. Thus the beam has a strong electric vector in the perpendicular direction.

C. Calibration of Filters and Determination of Effective Resolving Time of the Solid State Scintillation Detector

The multiple foil method of determining the effective resolving time of any counter is reliable. In this method the logarithm of the intensity (counting rate) of crystal-monochromatized x-ray transmitted by the absorbing foil is plotted as ordinate against the thickness of the foils. In the absence of coincidence losses this curve should be a straight line. Because of coincidence losses, the observed curve will fall below the true curve and the true curve is approximated by extrapolation from low intensities where the losses are negligible. The losses are taken to be the difference between the true counting rates and those determined experimentally. From these differences the effective resolving time τk is calculated using the formula,

$$\tau k = \left[\frac{I_{true}-I_{obs}}{I_{true} X I_{obs}}\right] \qquad (4)$$

A series of seven high purity filters with an average thickness of 0.0021 cm were prepared. Then all of them were positioned in front of the counter and copper K_α radiation was used. The transmitted intensities were varied by removing the filters one by one. The experimental values were plotted on a semi-log paper (Fig. 6), and it can be seen that the observed curve deviates from a straight line. The effective resolving time, found to be 21.05×10^{-6} sec (average), was calculated and is given in Table 1. In order to remain within the linearity of the electronic counting rates, the x-ray counting rates was always maintained below 5000 counts per second.

III. THEORY

Small angle scattering theory shows that, a medium containing a random distribution of electron density inhomogeneities will scatter incident x-ray radiation, according to the following expression,[10]

$$I(h) = I_e(h)\ N\ \overline{F^2(h)} \qquad (5)$$

Where,

$I_e(h)$ = coherent scattering of one electron

N = the number of inhomogeneities, irradiated

h = diffraction vector = $2\pi/\lambda\ (\underset{\sim}{S} - \underset{\sim}{S}_o) = 4\pi/\lambda \sin\theta$.

$F(h)$ = $\int_v \{\rho(r) - \rho_o(r)\} \exp(-\bar{h}\cdot\bar{r})\ dV$

$\rho(r)$ = the electron density of the inhomogeneity at r

$\rho_o(r)$ = the electron density of the matrix

dV = the volume of the inhomogeneities, i.e. the region in which $\rho(r)$ is different from $\rho_o(r)$.

2θ = the scattering angle

Therefore the intensity in electron units for an inhomogeneity (particle)

$$I_{eu}(h) = I(h)/I_e(h) = N\ F^2(h) = Nn^2\phi^2(h) \qquad (6)$$

n = number of electrons per particle. The particles are assumed identical in size and shape

$\phi^2(h)$ = the normalized intensity distribution function.

(1) The effective heterogeneity size parameter can be determined from the asymptotic curves of intensity verses scattering angle which shows subsidiary maxima and minima at angles related to the inhomogeneity dimensions. A useful approximation to the exact theory which holds very

well at the lowest angles has been found by Guinier[10]

$$I_{eu}(h) \underset{h\to o}{=} N n^2 \exp(-h^2R^2/3). \qquad (7)$$

where,

R = inhomogeneity radius of gyration, with electron density used as the analog of mass.

The approximation is always valid at small angle h, irrespective of particle shape and permits evaluation of the radius of gyration even in polydisperse systems.

(2) According to the Porod expression,[11] for the asymptotic curve at large h

$$\phi^2(h) \underset{h\to\infty}{=} 2\pi S/V^2h^4 \qquad (8)$$

where,

S = the total surface area of the particles

V = the volume of the heterogeneity

The curve ln $\phi^2(h)$ versus ln h has a limiting slope of -3 and ordinates proportional to S irrespective of the shape of the particles, when slit collimation is used.

IV. EXPERIMENTAL PROCEDURE

A. Materials

Pyrolytic graphite deposited at 2200°C was supplied by the Union Carbide Corporation. The as deposited density of the material is 2.20 gm/cm^3 which implies a porosity of the order of 4 percent when compared with the theoretical density of 2.29 gm/cm^3 for pure graphite.

Cleaved single crystals of LiF and specimens of high density polycrystalline graphite were chosen to study the specimen volume effect in the very ultra small angular region.

B. Specimen Preparation

Three pyrolytic graphite specimens approximately of 0.13 cmX1 cmX2 cm were cut so that the plane of the specimen was either parallel or perpendicular to the deposition surface (Fig.7). This is the optimum thickness for which the transmission is approximately 32% for maximum scattering. Similarly for Ni-filtered Cu-K_α radiation the optimum thicknesses for LiF single crystal and graphite are 18 mils and 56 mils respectively. For LiF and graphite four and five thicknesses were chosen very close to the optimum thickness to verify the volume effect. The LiF was cleaved along the (200) plane.

C. Small Angle Scattering

Small angle scattering was obtained by an AMR 6-220 x-ray low angle scattering Goniometer. Specimens were examined employing a Philips Standard Cu x-ray tube operated at 40 kv and 20 ma. A Phillips solid state detector, pulse height analyzer and scalar were also used for counting. X-ray counting rates were maintained below 5000 cps with

carefully calibrated Ni-filters (Table 1) in order to remain within the linearity of the electronics. All data were recorded employing an air path. The data were corrected for background by subtracting the scattering observed when the specimen was placed just in front of the detector, (that is the same absorption but with no scattering).

V. RESULTS AND DISCUSSION

The data were plotted on log-log plots as shown in Fig. 8 and 9. It is seen that at larger angles the average intensity has a limiting slope of -3 which is consistent with theory. In curves (a) and (b) the anisotropy in scattering is due to preferred orientation of pyrolytic graphite. Experiments showed that rotation of the specimen about the normal to the deposition plane gave results identical to those of Fig. 8a. This indicates that the inhomogeneous regions causing the small angle scattering are randomly oriented in the deposition plane as is observed for the crystallites in pyrolytic graphite.

In the small angular region, the scattering is very high for the orientation (c) and this curve has crossed the curve (b) at $h = 40 \times 10^{-4}$ in both Fig. 8 and 9. This excess scattering in curve Fig. 8(c) can be understood by reference to Fig. 10, where the data at small h are plotted as log intensity versus h^2. As shown in the theory, the Guinier approximation for a monodisperse system of particles applies at small h. Thus since the measurements pertain to the same volume of the same material, both the curves (a) and (c) in Fig. 10 should extrapolate to the same intercept at the origin irrespective of orientation. This excess scattering above the extrapolated line is ascribed to double Bragg scattering.

As pointed out by Warren,[12] there is a possibility of strong double Bragg scattering reflection due to correlation in the orientation of the individual crystals. In discussing the small angle scattering resulting from cold worked metals, it is assumed that the original crystals of average dimensions $\langle G \rangle$ are broken up into a large number of small subgrains

with slightly varing orientations. The diffracted beam from one of these subgrains then traverses an average distance ⟨ D ⟩ through the other subgrains of the original grain. Since these subgrains all have nearly the same orientation, there is a much higher probability for a second reflection in other subgrains. In pyrolytic graphite, the crystallites have layer planes tilted at an average angle 'α' away from the original deposition surface and because there is no preferred orientation in the deposition plane of the deposited material, the double Bragg scattering will be possible from (0002) planes, like cold worked metals. As shown by Bragg and Packer[13] the orientation distribution of pyrolitic graphite is essentially $\exp(-K\alpha^2)$ with $K \sim 5$ for 2200°C deposition and the fraction of crystallites having normals oriented at an angle 'α' relative to the deposition plane is $\cos \alpha/2$ for random orientation.

Thus refering all angles to the normal to the deposition surface, with x-ray beam having the electric vector parallel to the layer planes, for Fig. 7c, the relative orientation is,

$$\frac{\exp(-K\alpha^2)}{\sin\frac{\alpha}{2}} = \frac{\exp\left[-5\times\left(\frac{13.3\times\pi}{180}\right)^2\right]}{\sin\frac{(13.3)}{2}} = \frac{0.763}{0.115} = 6.6 \text{ times random.}$$

In this case 'α' is taken as θ corresponding to (0002) which is 13.3°. For the other two orientations, Fig. 7a and b, with electric vector perpendicular to the layer planes, the relative orientation is

$$\frac{\exp\left[-5\times\left\{\frac{(90-13.3)\pi}{180}\right\}^2\right]}{\cos\frac{\alpha}{2}} = \frac{\exp(-9)}{\cos\frac{13.3}{2}} = 2.54\times10^{-4} \text{ times random}$$

Thus the degree of randomness for the orientation in Fig. 7c is much higher than the orientations in (a) and (b). Therefore it can be expected that a strong double Bragg scattering should occur only in (c) and essentially none in (a) and (b). Secondly, if we compare the shape of the three curves, (a) and (b) are approximately similar whereas curve (c) is quite different from them which is due to double Bragg scattering. By using unpolarized beams double Bragg scattering, which was due to the horizontal electric vector of the x-ray beam, was observed in the orientation (b).[3] But in this experimental work, double Bragg scattering has been eliminated in this orientation by using a strongly polarized beam.

In the ultra small angular region, the unexpected increase in scattering intensity was observed which did not obey the Guinier approximation. Assuming this to be due to the volume of the specimen, two experiments with LiF (single crystal) and pure graphite were performed and the results are shown in Fig. 11 and 12. In both the specimens, it was found that with decrease in thickness, with specimens beginning above the optimum thickness, the intensity always increased in LiF, contrary to what would be expected, Fig. 11, i.e. it should decrease with decrease in thickness. However, in the case of pure graphite, the intensity increased with decrease in thickness up to 60 secs of θ, as in the case LiF. Thereafter it increased with increase in thickness. These experimental results can be clearly understood taking into account the volume effect. In the case of graphite, the increase in intensity with increase in thickness, in the large angular region was due to small angle scattering by voids, and the volume effect was negligible. But since the LiF

(single crystal) did not give any measurable small angle scattering, the curves did not converge. Furthermore the Guinier approximation was not valid in the ultra small angular region, which shows that the increase in scattering was due to volume of the specimen.

Theoretically an expression was derived by Guinier taking into account the Fraunhofer approximation where the intensity is stated to be directly proportional to the square of the volume of the material,[14] but our results demonstrate that this is not true. Later on, Warren[6] pointed out that the intensity in this small angular region observed in practice results from Fresnel diffraction, which is consistent with our experimental results.

VI. CONCLUSIONS

In pyrolytic graphite, double Bragg scattering has been observed when the electric vector was parallel to the deposition plane. No such effect was observed in other two orientations. Thus, it was found that double Bragg scattering can be eliminated in certain orientation by using polarized beam.

In the very small angular region, an apparently anomalous increase in scattered intensity was found to be due to the volume of the material, which most likely is due to Fresnel diffraction instead of Fraunhofer diffraction. A theory must be worked out to study and correlate this effect.

ACKNOWLEDGEMENTS

The author is deeply grateful to Professor Robert H. Bragg for his guidance and encouragement throughout this investigation. Thanks are also due to Professor Richard M. Fulrath for having supplied the material used in this investigation.

This work was done under the auspices of the Unites States Atomic Energy Commission through the Inorganic Materials Research Division of the Lawrence Radiation Laboratory, Berkeley, California.

APPENDIX A

When a x-ray beam strikes the Ge crystal plane, it is partially polarized owing to the reflection by the crystal. Considering the intensity of an unpolarized beam as the sum of two equal parts due to independent components in two orthogonal directions of polarization, (Fig. 13)

$$I_o = I_p + I_n$$

or

$$1/2\ I_o = I_p = I_n \qquad (1)$$

where I_o = intensity of the unpolarized beam

'p' indicates the component in the plane of incidence and 'n' is the component perpendicular to it. Using the amplitude of the optical field, equation (1) can be written as:

$$1/2\ E_o^2 = E_p^2 = E_n^2 \qquad (2)$$

Taking the 'p' component first, this component is reflected by the Ge crystal plane at P_1 (whose normal N_1 lies in the xy plane) along y' direction (also lying in the xy plane) which is inclined by 2θ to y (Fig. 14). After reflection the 'p' component becomes

$$E'_p = k\ E_p \cos 2\theta \qquad (3)$$

where, $k = (e^2/mc^2r)$ and contains all the factors which are independent of the direction of polarization. This component also lies in the xy plane and parallel to the x-axis.

This component is next reflected by the second plane of the grooved Ge crystal to the first plane at the point P_2 along y" which is also

inclined at an angle 2θ to the y' direction (again parallel to y) because the two planes in the grooved crystals are parallel. Therefore,

$$\begin{aligned} E'' &= k\, E'_p \cos 2\theta \\ &= k^2 E_p \cos^2 2\theta \end{aligned} \tag{4}$$

Repeating the above procedure, after six reflections,

$$E_p^{vi} = k^6 E_p (\cos^6 2\theta)$$

therefore

$$I_p^{vi} = (E_p^{vi})^2 = k^{12} E_p^2 \cos^{12} 2\theta = k^{12} E_o^2 \cos^{12} 2\theta \tag{5}$$

Similarly, the 'n' component which is not affected after reflection by the plane at P_1

$$E'_n = k\, E_n \tag{6}$$

After six reflections,

$$\begin{aligned} E_n^{vi} &= k^6 E_n \\ I_n^{vi} &= (E_n^{vi})^2 = k^{12} E_o^2 \end{aligned} \tag{7}$$

Taking the ratio of (7 and 5 and substituting the value of $2\theta = 45.3°$ for Ge (220) planes,

$$\frac{I_n^{vi}}{I_p^{vi}} = \frac{k^{12} E_o^2}{k^{12} E_o^2 \cos^{12} 2\theta} = \frac{1}{(\cos 45.3)^{12}} = 68 \tag{8}$$

Equation 8 shows that the intensity in the perpendicular direction is 68 times greater than the intensity in horizontal direction. Thus a highly polarized beam is obtained after 6 reflections, having electric vector parallel to the reflecting planes.

REFERENCES

1. A. R. Brown and W. Watt, Industrial Carbon and Graphite, 58 (Soc. Chem. Indust. London, 1958).
2. O. J. Guentert and S. Cvikevich, Proc. 5th Carbon Conf. 1(1961) 473 (Pergamon Press, Oxford, 1962).
3. R. H. Bragg, M. L. Hammond, Nature, 1963, 200 p. 555.
4. U. Bonse, and M. Hart, Applied Physics Letters, 7 : 238 (1965).
5. A. Guinier and Fournet, Small Angle Scattering of X-Ray (John Wiley and Sons, New York, 1955).
6. B. E. Warren, "Small Angle Scattering from Large Volumes,"
7. U. Bonse and M. Hart, Applied Physics Letters 7, 238 (1965).
8. A. Guinier and Fournet, Nature, 160, 501, (1947).
9. D. Mond, Phys. Rev. 72, p. 83 (1947).
10. A. Guinier and Fournet, "Small Angle Scattering of X-rays" p. 119.
11. W. S. Rothwell, J. of Applied Phys. 12, 837 (1959).
12. B. E. Warren, Acta. Cryst. 12, 837 (1959).
13. R. H. Bragg and V. M. Parker, Nature 195, 1080 (1962).
14. A. Guinier and Fournet, "Small Angle Scattering of X-Rays", John Wiley and Sons, New York, 1955, p. 39).

Table I

$I_{trans.}$ Counts/secs.	$I_{obs.}$ counts/sec.	$k = \frac{I_{trans} - I_{obs}}{I_{trans} \times I_{obs}}$
29,000	17.800	21.70×10^{-6}
30,000	19,500	18.00×10^{-6}
35,000	20,000	20.00×10^{-6}
45,000	21,500	24.30×10^{-6}

FIGURE CAPTIONS

Fig. 1. Multiple reflection within a groove cut into a Ge crystal. The beam is again parallel to the primary beam after six times reflected within the groove.

Fig. 2(a). Calculated rocking curve for (200) reflection in Si perfect crystal. Five consecutive Bragg reflections yield much steeper reflection characteristic R^5.

Fig. 2(b). Observed rocking curve after twelve reflections from Ge crystal without any specimen and at zero angle of 2θ.

Fig. 3(a). Small angle scattering photogram at the specimen position which shows a strong line in the center with gradual decrease in intensity in both sides of the strong line.

Fig. 3(b). Intensity distribution across the equator (perpendicular bisector of the primary beam image) of the film. This is determined with a microphotometer of scanning area 2 mm×200 micron.

Fig. 4(a). Small angle scattering photogram at the detector position.

Fig. 4(b). Intensity distribution across the equator of the film at the detector position. This is also determined with a microphotometer of scanning area 2 mm×200 microns.

Fig. 5. Trace of the primary beam on the film. P is the point on the film equator.

Fig. 6. Intensity versus thickness of the nickel filters. Linearity can be maintained within 5000 counts per second.

Fig. 7. Three pyrolytic graphite specimen having different orientations with x-ray beam. The basal plane in (a) and (c) are parallel to electric vector whereas in (b) it is perpendicular.

Fig. 8. Log-log plot of small angle scattering curves in three different orientations. Thickness of the specimen is 0.130 cms.

Fig. 9. Log-log plot of small angle scattering curves in three different orientations. Thickness of the specimen is 0.125 cms.

Fig. 10. Guinier plot for the orientations (a) and (c) from Fig. 8. Excess scattering above the dashed line is due to double Bragg scattering in curve (c).

Fig. 11. Scattering in the small angular region in LiF single crystal with four different thicknesses. The scattering is due to volume of the specimen and the scattering increases with decrease in thickness.

Fig. 12. Scattering in the small angular region in graphite for five different thicknesses. In this case the scattering increases with decrease in thickness in small angular region.

Fig.13(a). The electric and magnetic field vectors of a linearly polarized x-ray wave lie in two orthogonal planes.

(b). Only the electric field distribution is used for describing the state of polarization.

(c). Reflection of polarized x-ray. The two orthogonal components are oriented perpendicular and parallel to the plane of incidence and denoted by subscript 'n' and 'p'.

Fig. 14. Intensity of the unpolarized beam after reflection in the first plane at F_1 and then again at the second plane at the point P_2.

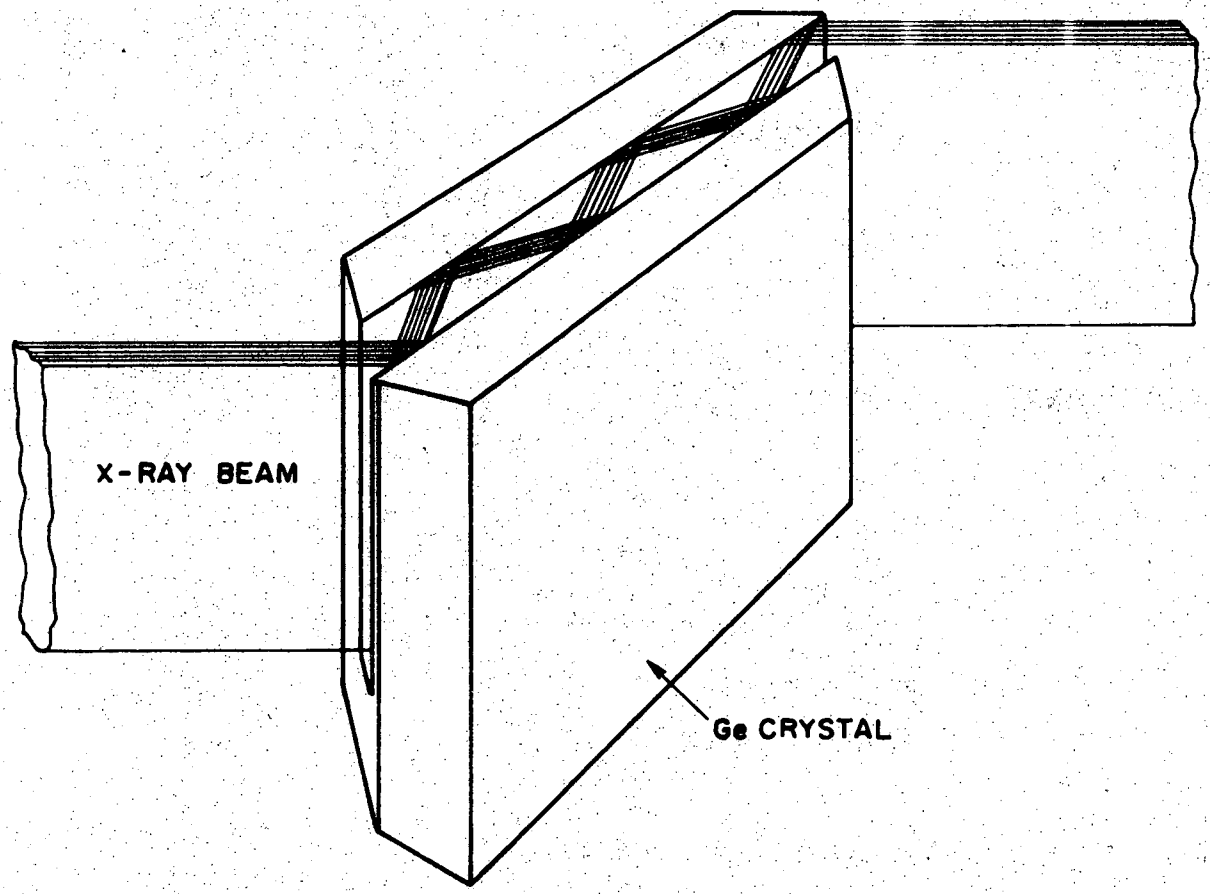

XBL 711-6447

Fig. 1

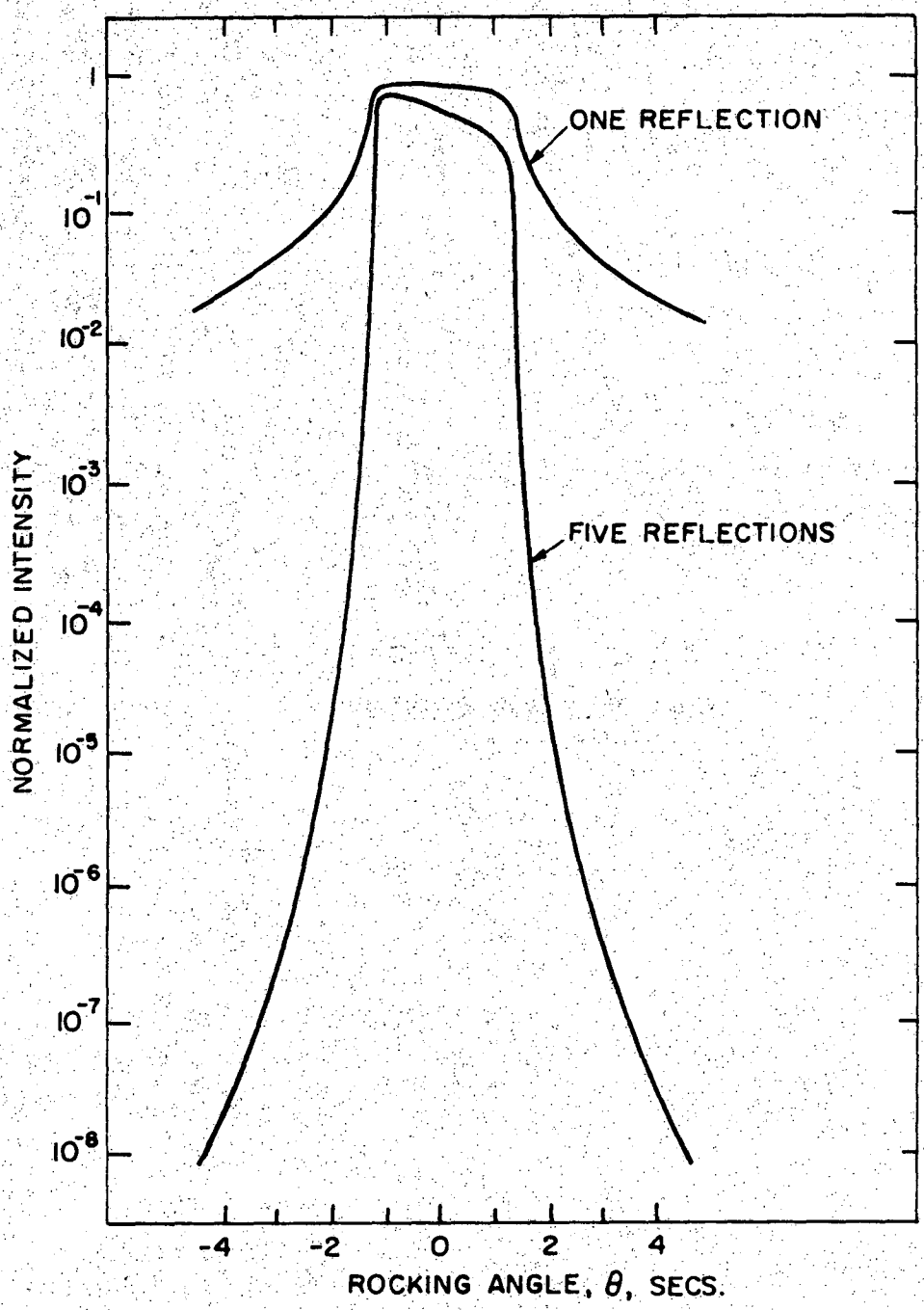

XBL711-6448

Fig. 2(a)

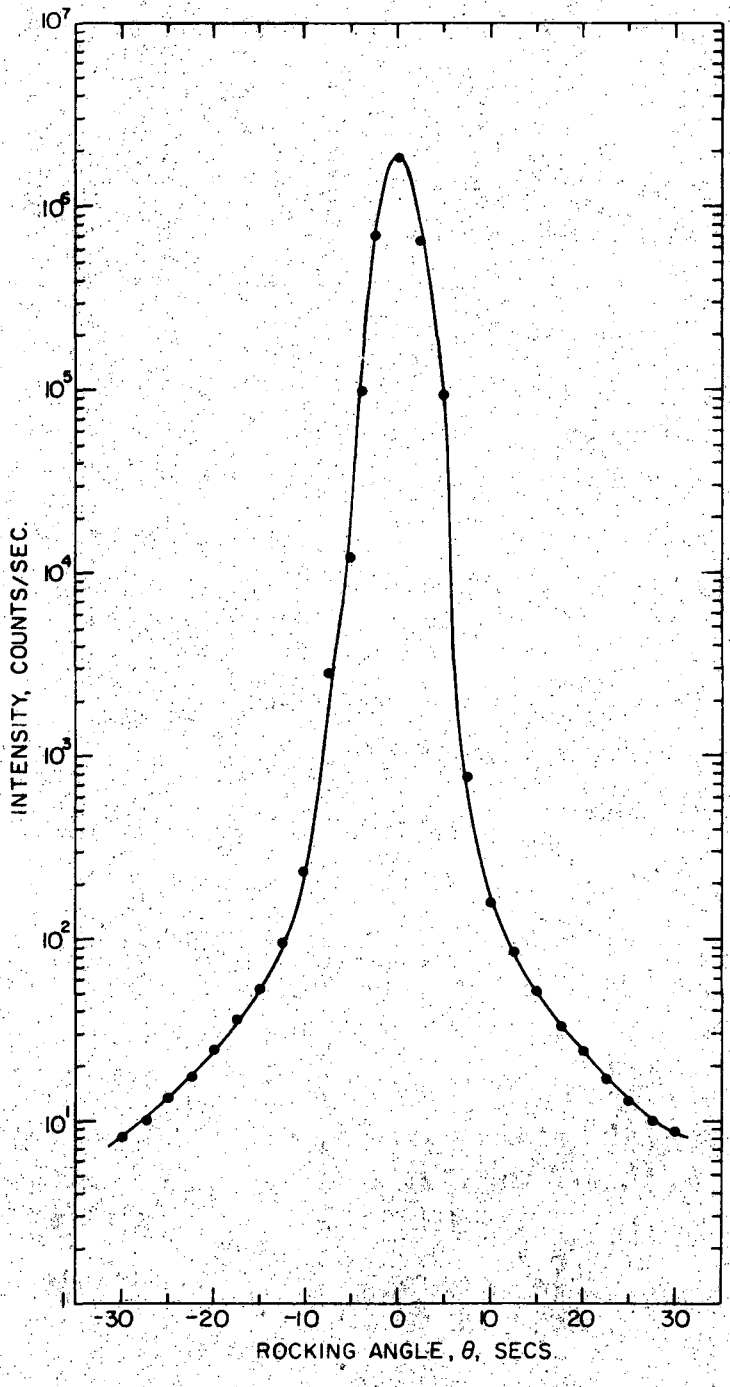

XBL711-6449

Fig. 2(b)

Fig. 3(a)

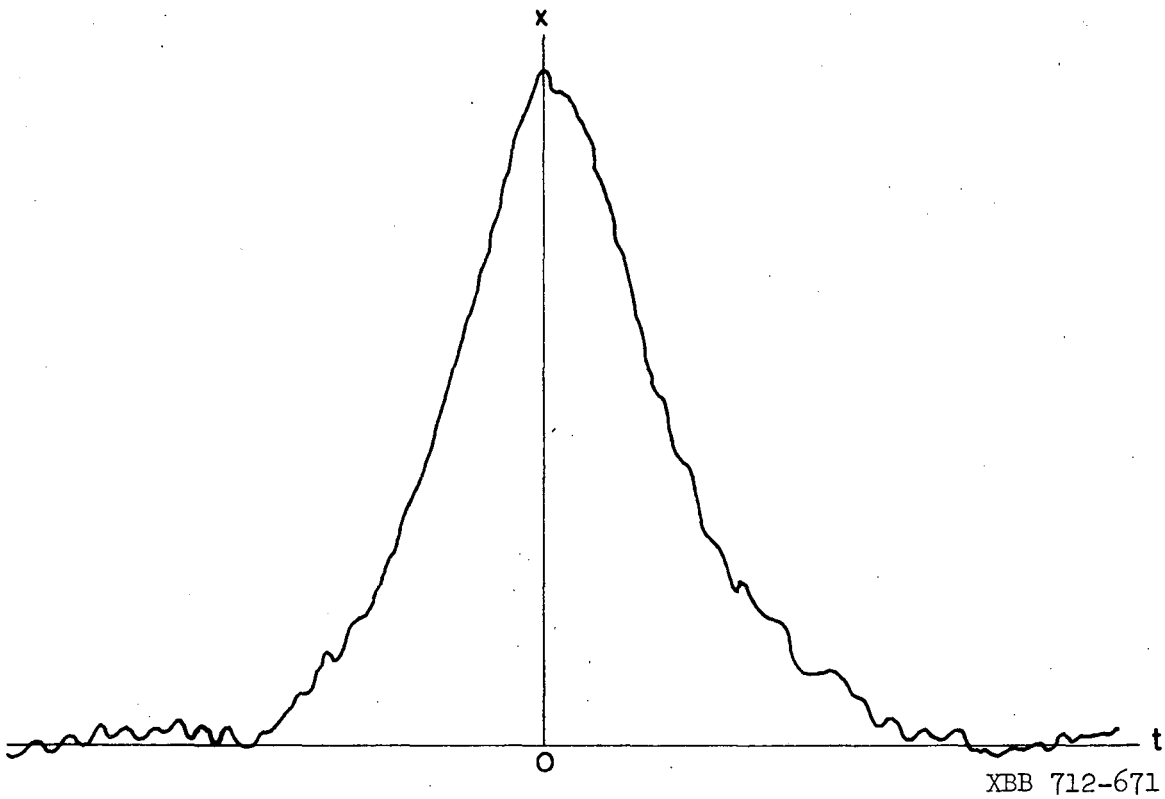

Fig. 3(b)

Fig. 4(a)

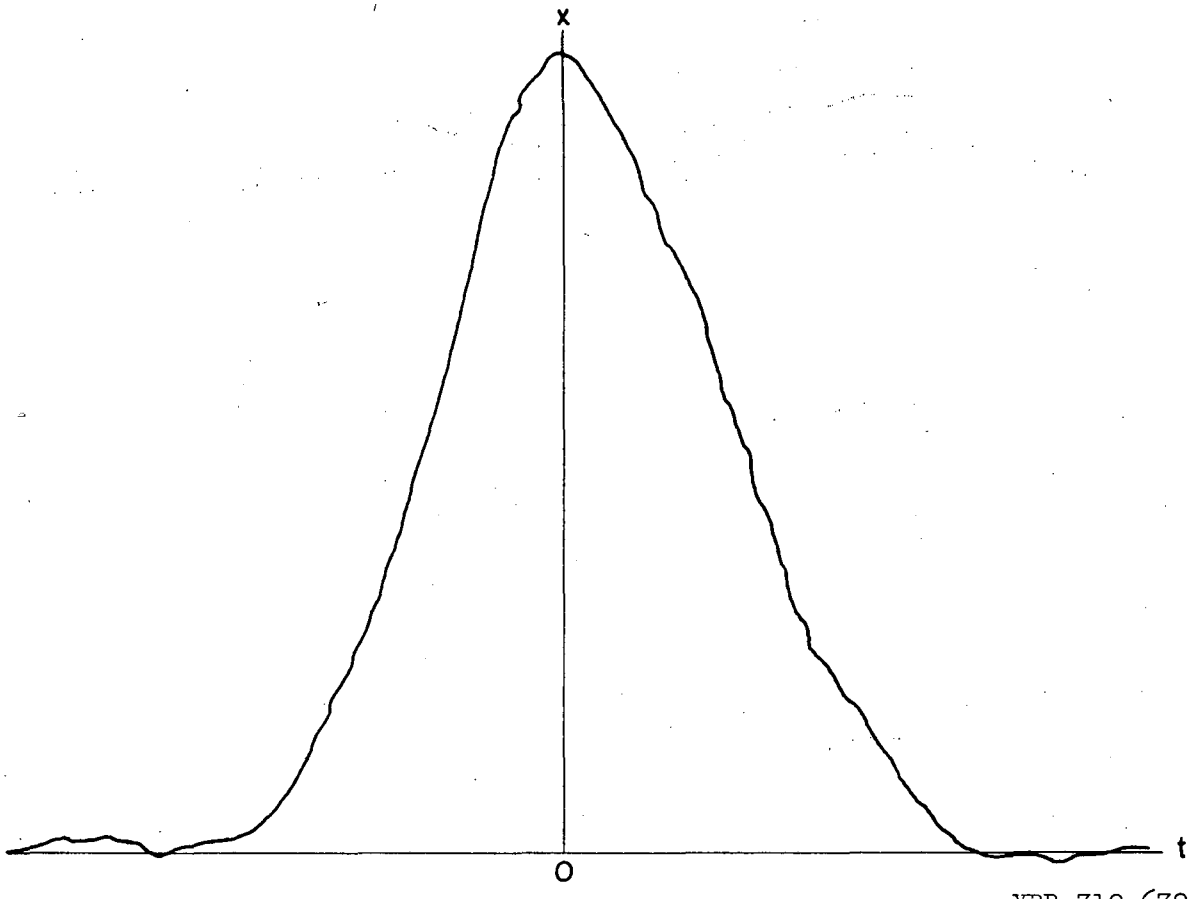

XBB 712-672

Fig. 4(b)

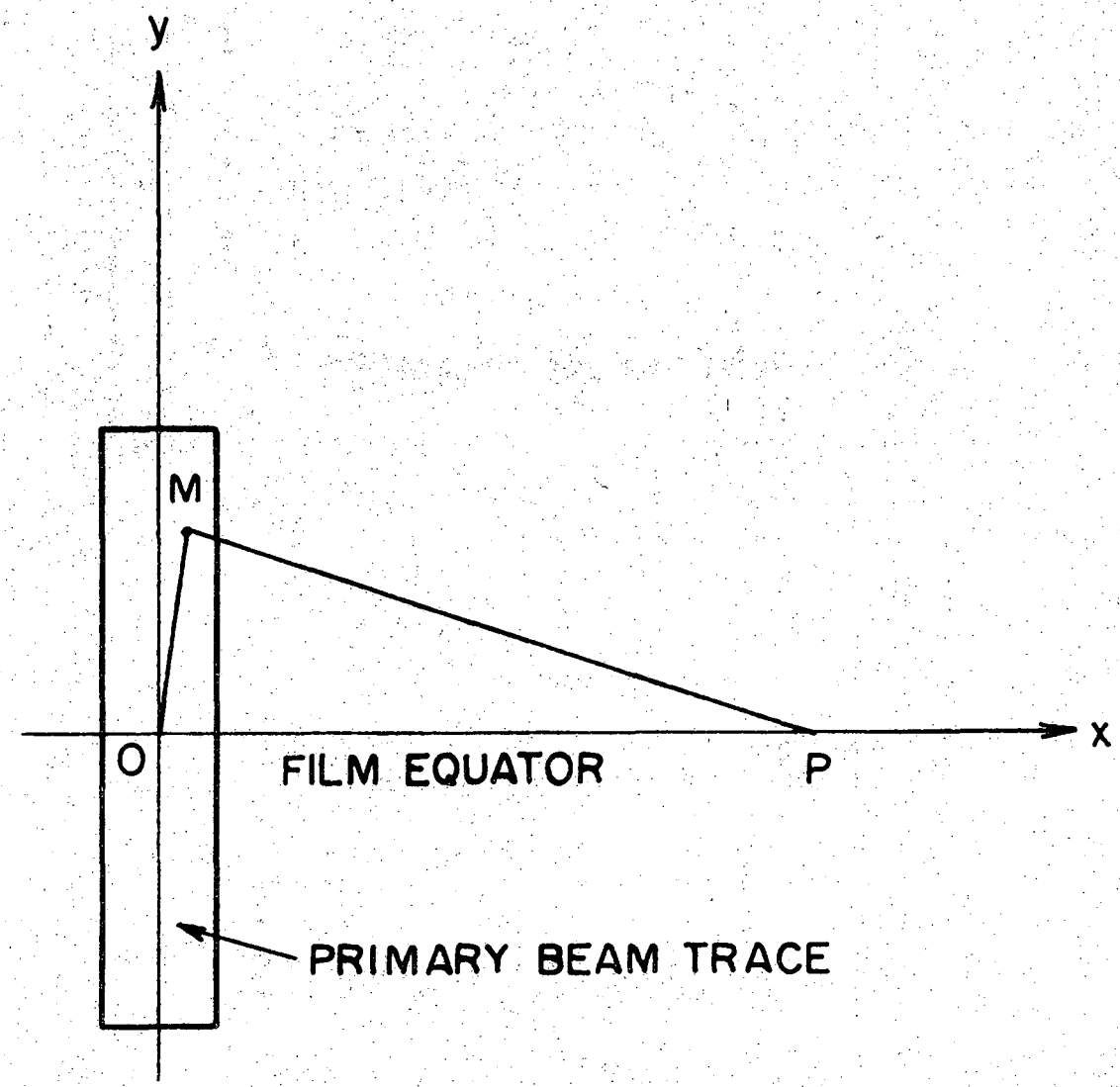

XBL711-6452

Fig. 5

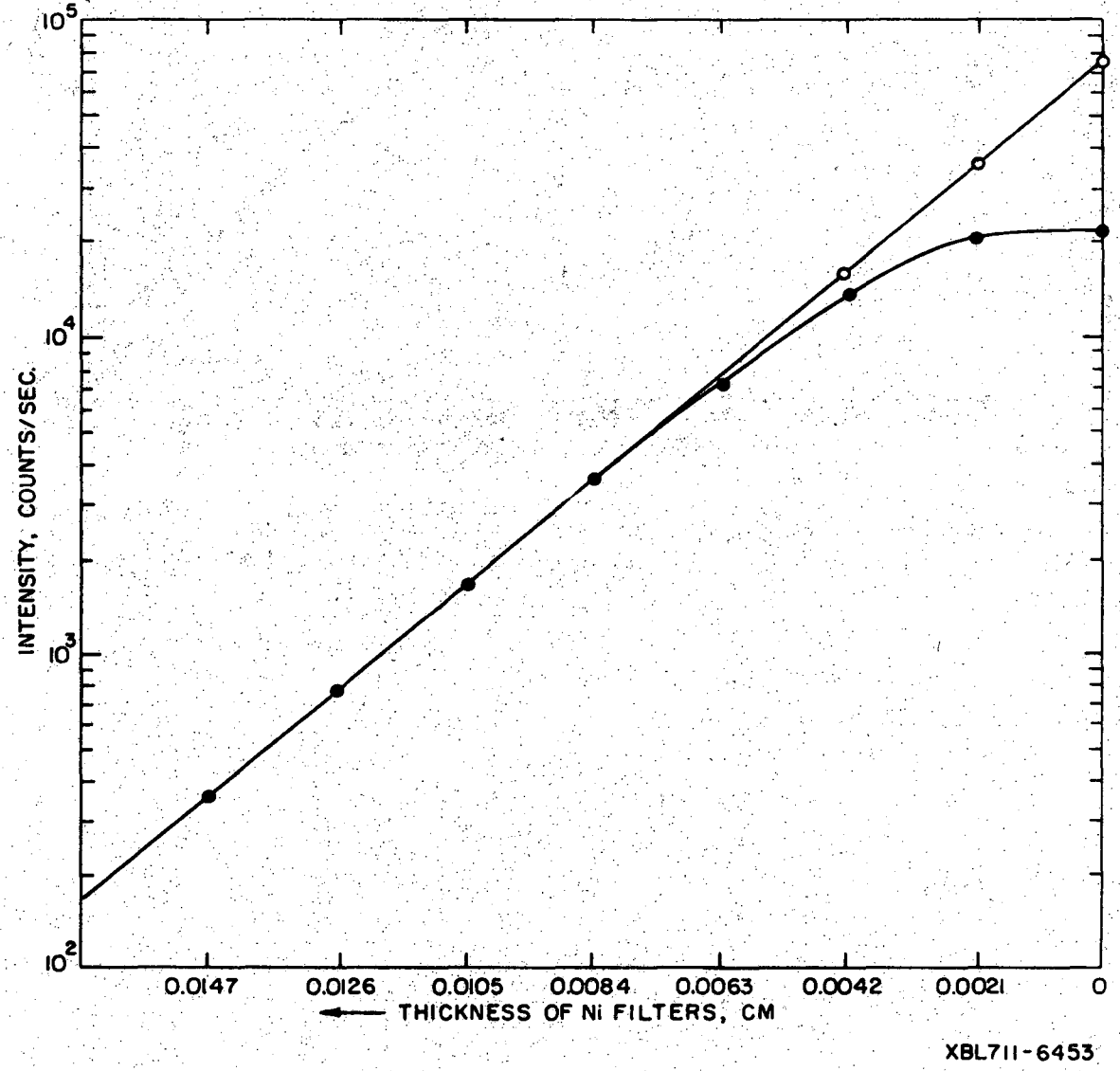
10^5
10^4
10^3
10^2
INTENSITY, COUNTS/SEC.
0.0147
0.0126
0.0105
0.0084
0.0063
0.0042
0.0021
0
THICKNESS OF Ni FILTERS, CM
XBL711-6453

Fig. 6

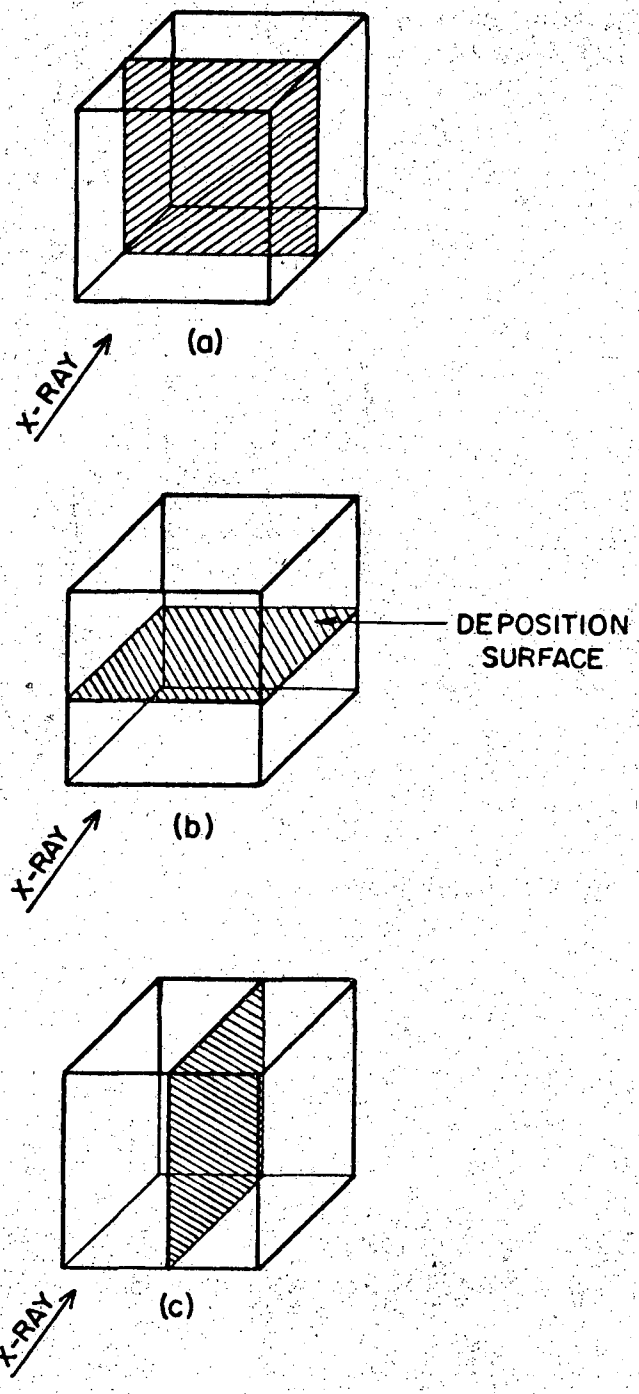

XBL711-6454

Fig. 7

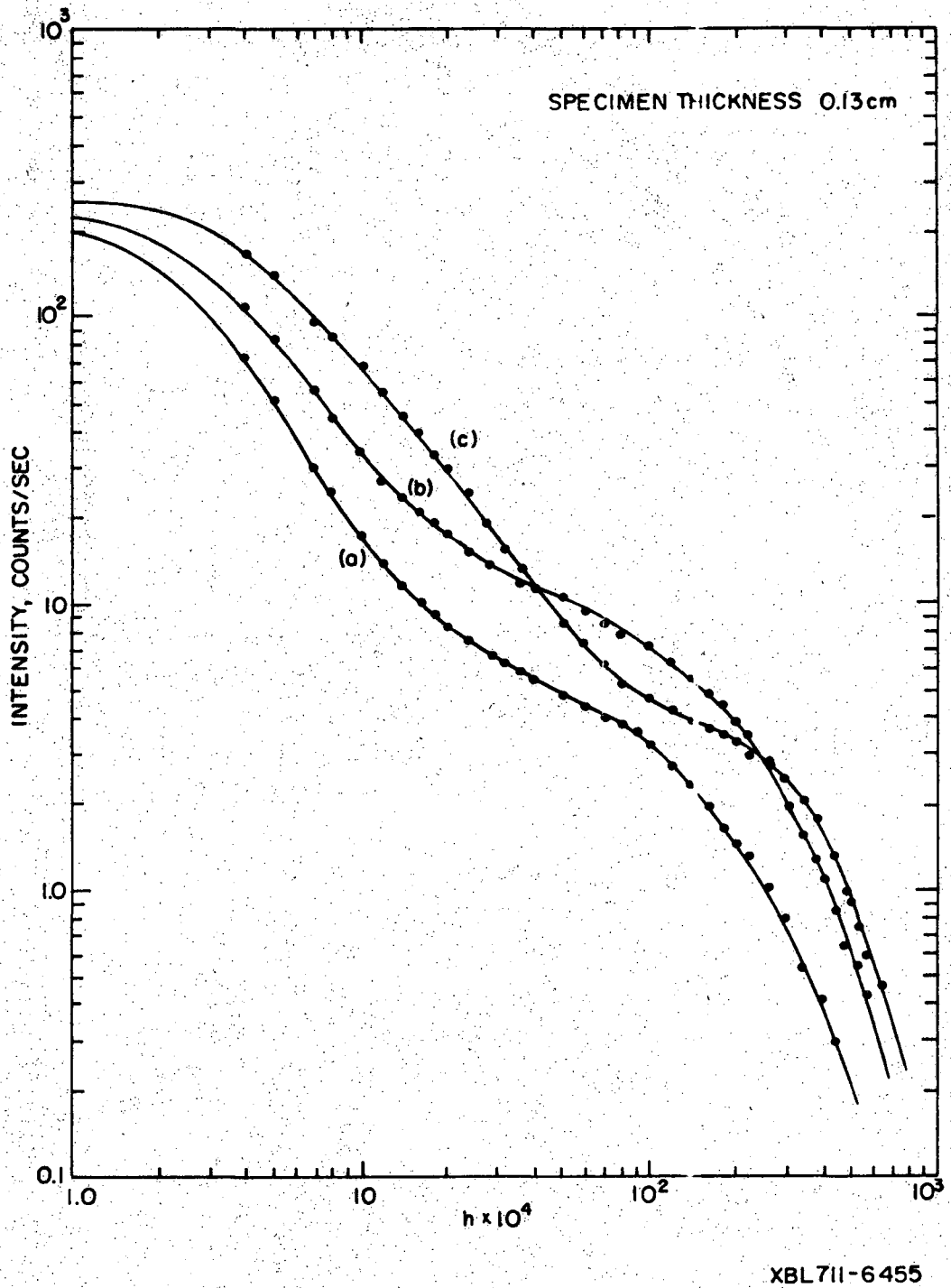
SPECIMEN THICKNESS 0.13cm
INTENSITY, COUNTS/SEC
h x 10⁴
(a)
(b)
(c)
10³
10²
10
1.0
0.1
1.0
10
10²
10³
XBL711-6455

Fig. 8

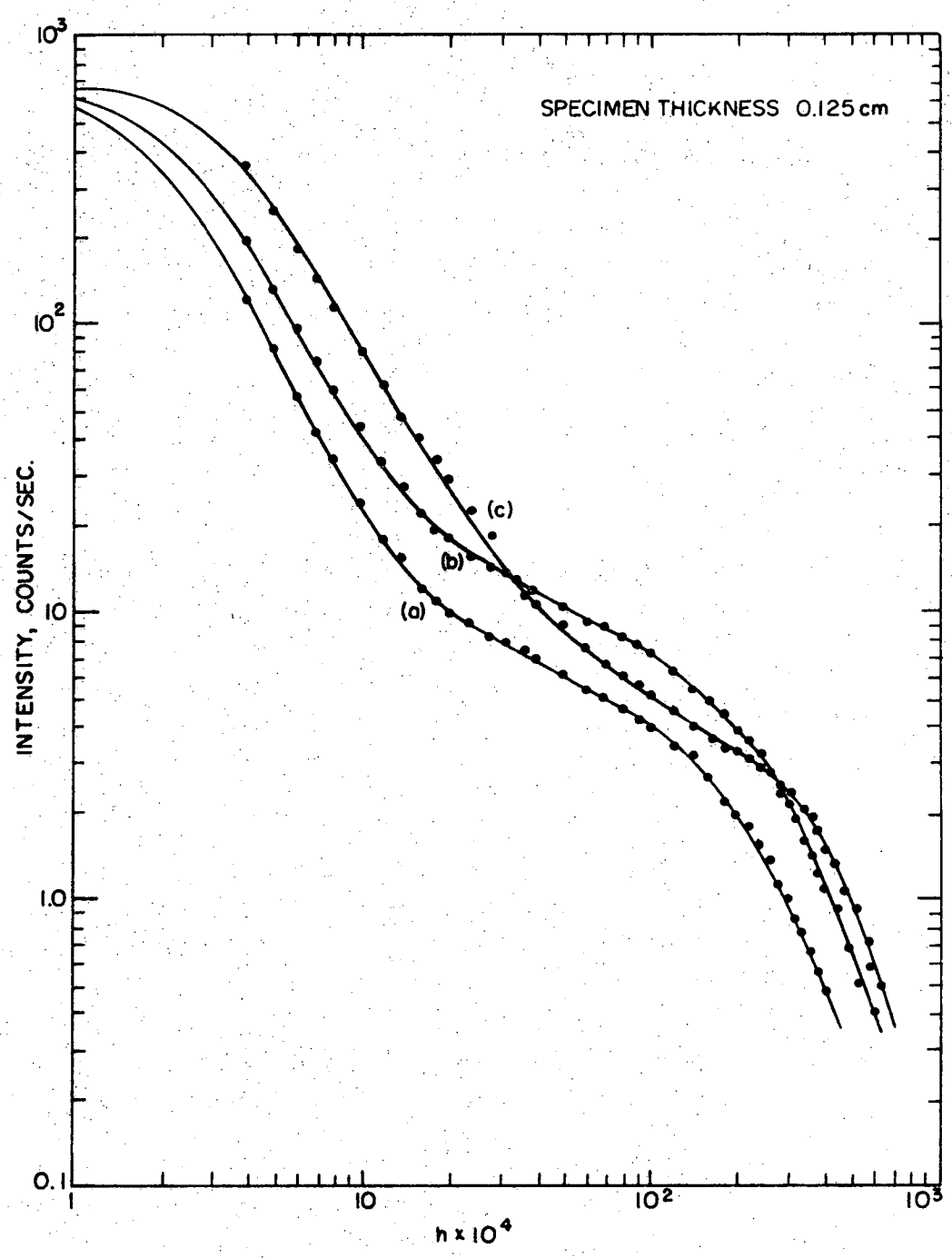

XBL711-6456

Fig. 9

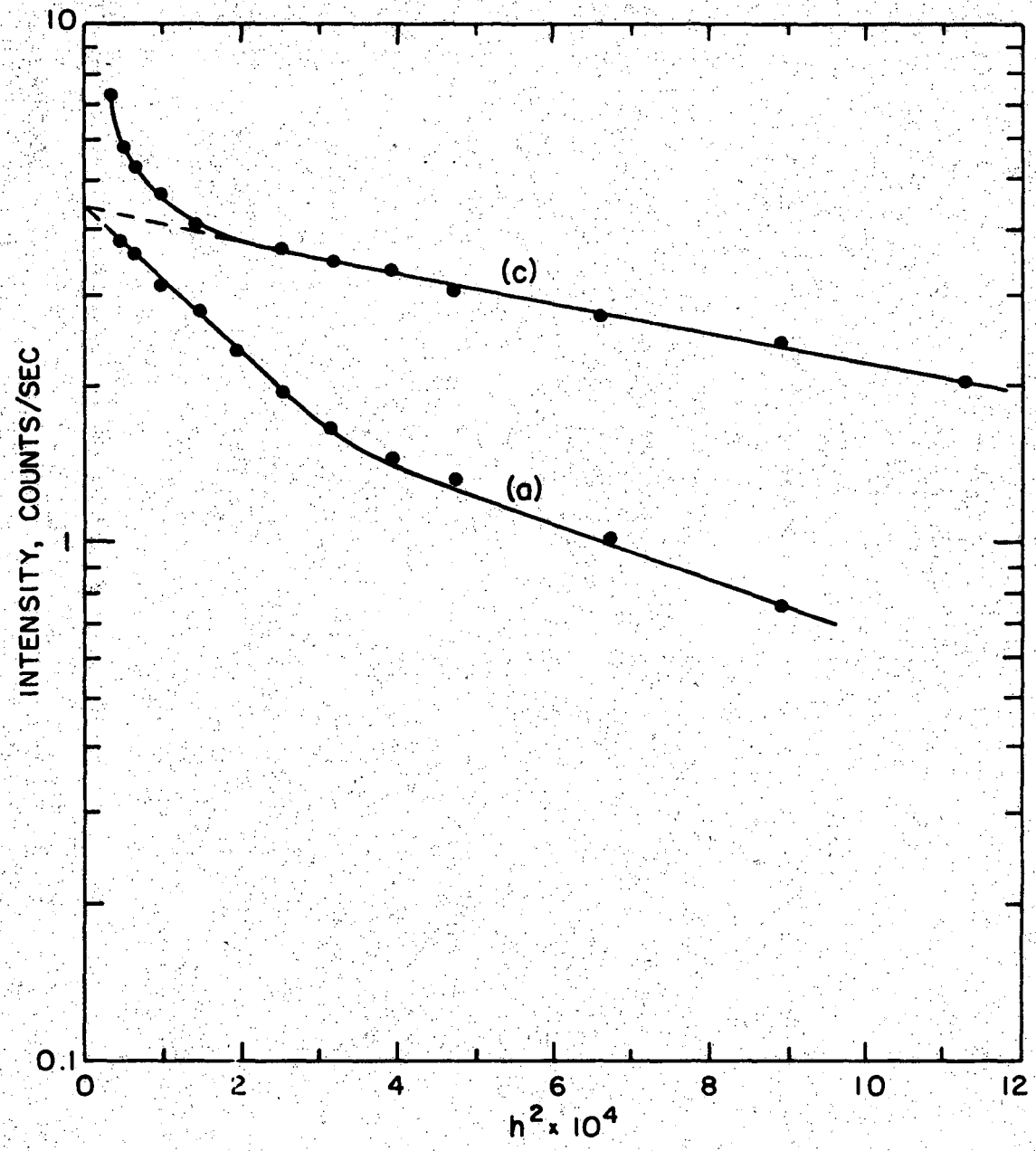

XBL711-6462

Fig. 10

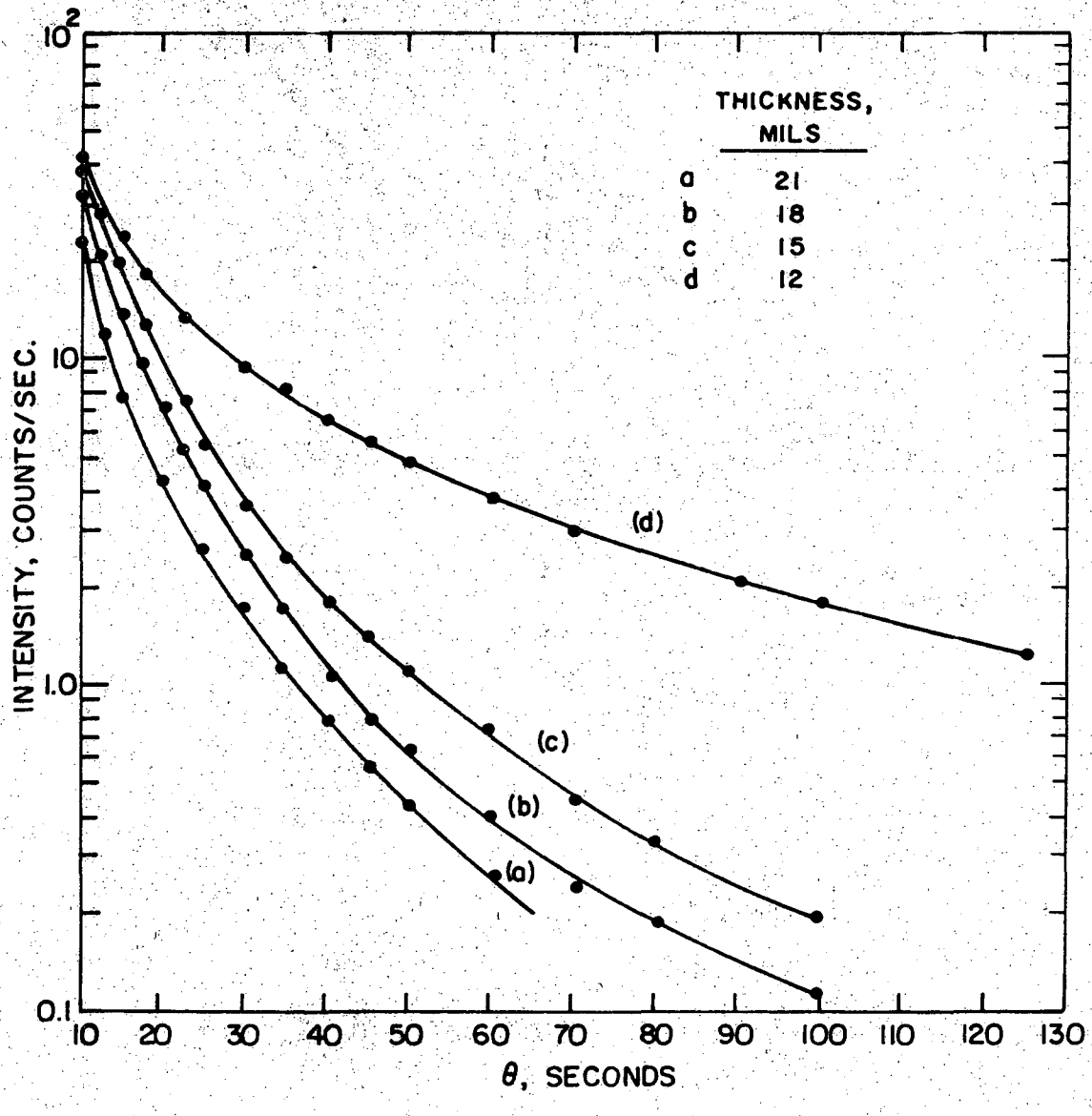

XBL711-6457

Fig. 11

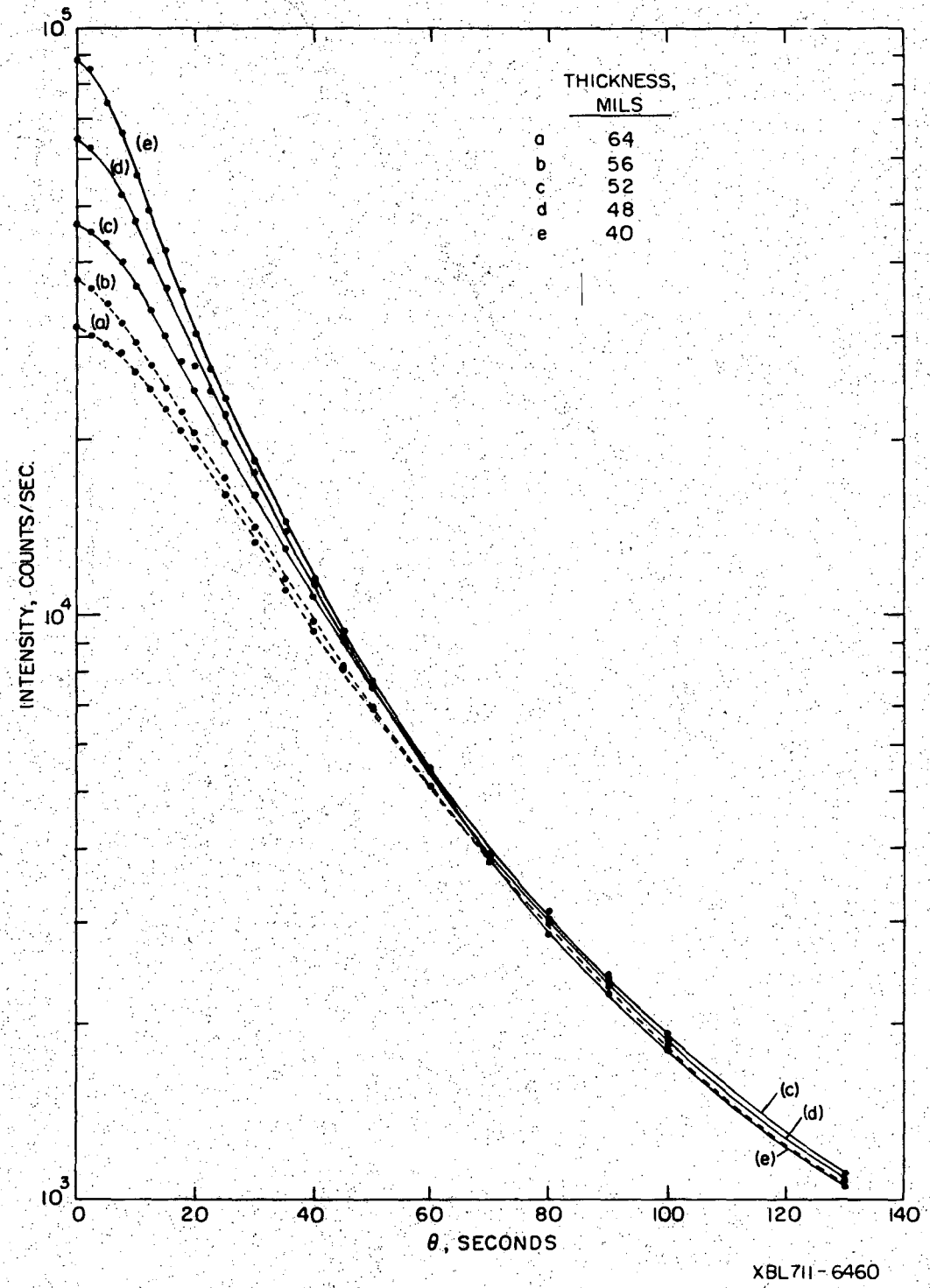
THICKNESS, MILS
a 64
b 56
c 52
d 48
e 40
(a)
(b)
(c)
(d)
(e)
INTENSITY, COUNTS/SEC.
θ, SECONDS
XBL711-6460

Fig. 12

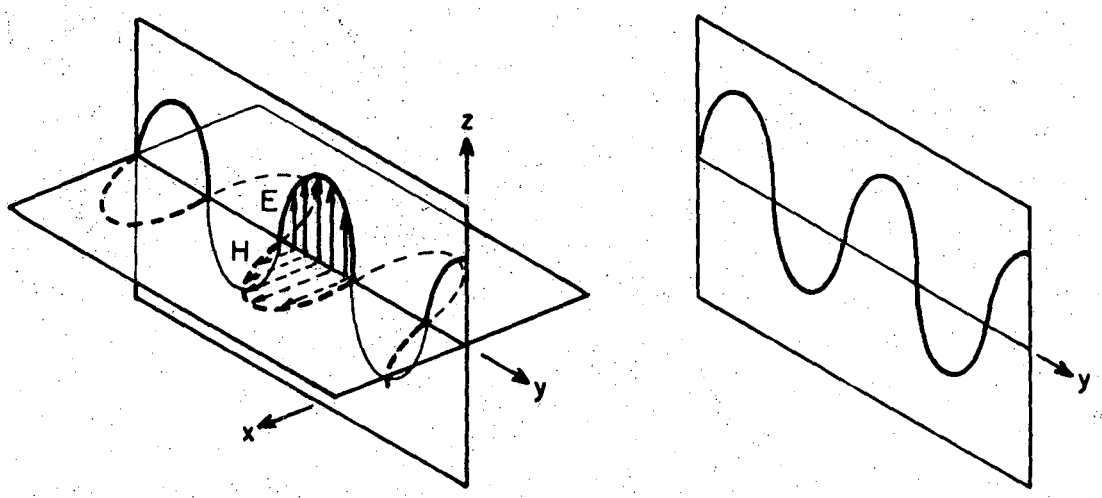

(a)

(b)

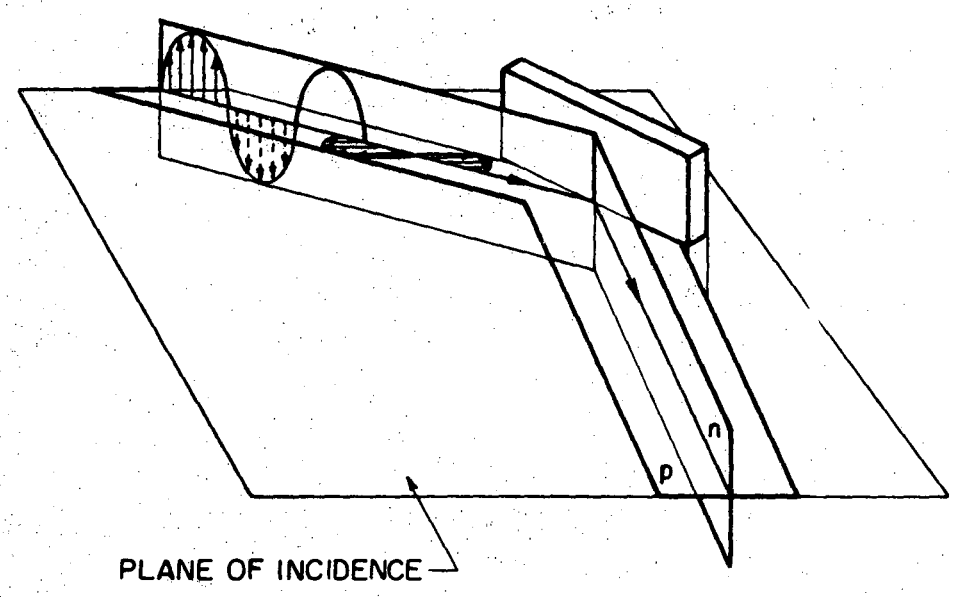

(c)

XBL711-6458

Fig. 13

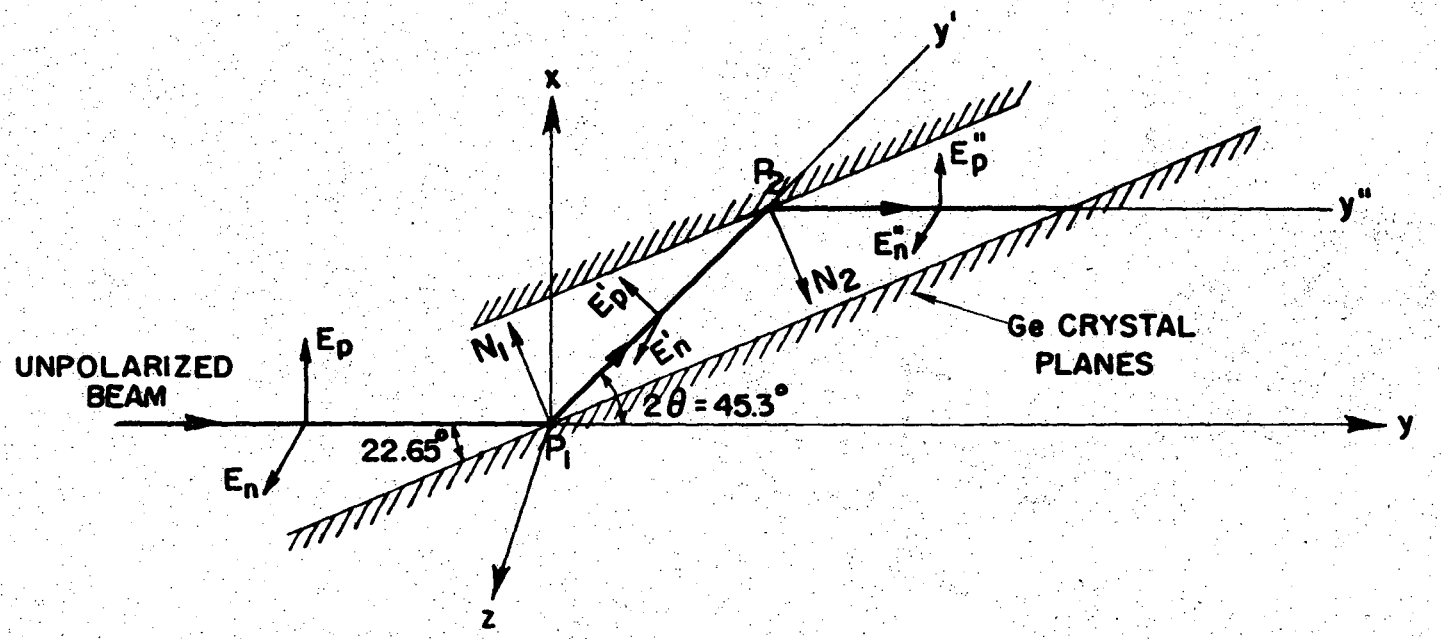

XBL711-6459

Fig. 14

TECHNICAL INFORMATION DIVISION
LAWRENCE RADIATION LABORATORY
UNIVERSITY OF CALIFORNIA
BERKELEY, CALIFORNIA 94720